Engineering Structures 32 (2010) 922–932

Contents lists available at ScienceDirect

Engineering Structures

journal homepage: www.elsevier.com/locate/engstruct

Strength prediction of squat structural walls via calibration of a shear–flexure interaction model

Leonardo M. Massone *

Department of Civil Engineering, University of Chile, Blanco Encalada 2002, Santiago, Chile

ARTICLE INFO

Article history:
Received 24 June 2009
Received in revised form
9 October 2009
Accepted 8 December 2009
Available online 12 January 2010

Keywords:
Shear strength
Squat wall
Reinforced concrete
Experiment
Interaction model
Calibration
Flexure
Shear

ABSTRACT

This study deals with a modeling approach that integrates shear and flexure interaction to predict the response of reinforced concrete squat walls. The model incorporates RC panel behavior into a displacement-based column model by prescribing the average horizontal strain, at different wall heights, which is calibrated using a 2D finite element formulation model (2D-FEM) that incorporated identical RC panel behavior. Experimental evidence shows relatively good correlation of the maximum and distribution over the wall height of the average horizontal strain prediction, with drift variation. The model shear strength was also compared to a database of 252 specimens, resulting in an average ratio of the predicted over the experimental shear strength (V_{model}/V_{exp}) of 1.13 for all the cases, with a coefficient of variation of 0.25, indicating a reasonably good correlation with the tests results. A sensitivity study indicates that the model strength prediction ratio, that is, the model over the experimental strength value, is almost nil sensitive to the vertical and horizontal web reinforcement strength ratio, as well as the longitudinal boundary reinforcement strength ratio, cross-sectional shape (rectangular or enlarged section), boundary condition (cantilever or fixed-end condition) and the axial load level supporting the reliability of the model.

1. Introduction

Walls are commonly used in structural configurations that require strong and stiff elements. In low-rise constructions or in long walls with perforations for window and door openings, short or squat walls (with aspect ratios typically less than 1.5) are found. Current design approaches, such as ACI 318-08 (Section 21.9) [1], promote a seismic design that prevents shear failure, in favor of a more ductile behavior like, flexural failure. When short or squat walls are considered, applied shear forces tend to control the wall response over applied moments, which explains common shear cracking or shear failure in these types of elements. In such cases, to promote flexural yielding, shear strength prediction becomes significant. On the other hand, in structural buildings the distribution of forces also necessitates a reasonable estimate of element stiffness values, as is also the case for structural walls. Therefore, a model capable of accurately determining strength and stiffness is desirable in design.

Although separating the flexural and shear behaviors is common practice, experimental evidence revealed that flexural and shear deformation interaction exists even for relatively slender walls dominated by flexural yielding (aspect ratio of three to four), resulting in nonlinear shear deformations contributing to approximately 10% of the roof level lateral displacement, and with an even higher degree of lateral displacement contribution at the plastic hinge zone [2].

The simplicity of formulating a column-type element, such as a displacement-based element makes it more suited to system studies, and therefore for implementation in computational platforms, which engineers could use to model and design structural walls. Thus, a simple, column-type modeling approach capable of incorporating shear–flexure interaction, originally calibrated for a limited number of wall tests, is generalized within a wide range of wall parameter values using analytical results from a 2D finite element formulation (2D-FEM). The overall load–displacement response is compared with selected experimental results. The model lateral strength is also compared with a large database of 252 wall specimens.

2. Research significance

Low aspect ratio reinforced concrete walls are common in low-rise and perforated wall-type construction. Accurate modeling of the load vs. deformation response and particularly the capacity estimation of wall elements are essential in wall design. A column-type model that captures coupling of shear–flexure behavior is calibrated using expressions obtained by a 2D-FEM model utilizing identical material properties, and model results are validated by

* Tel.: +56 2 9784984; fax: +56 2 6892833.
E-mail address: lmassone@ing.uchile.cl.

0141-0296/$ – see front matter
doi:10.1016/j.engstruct.2009.12.018

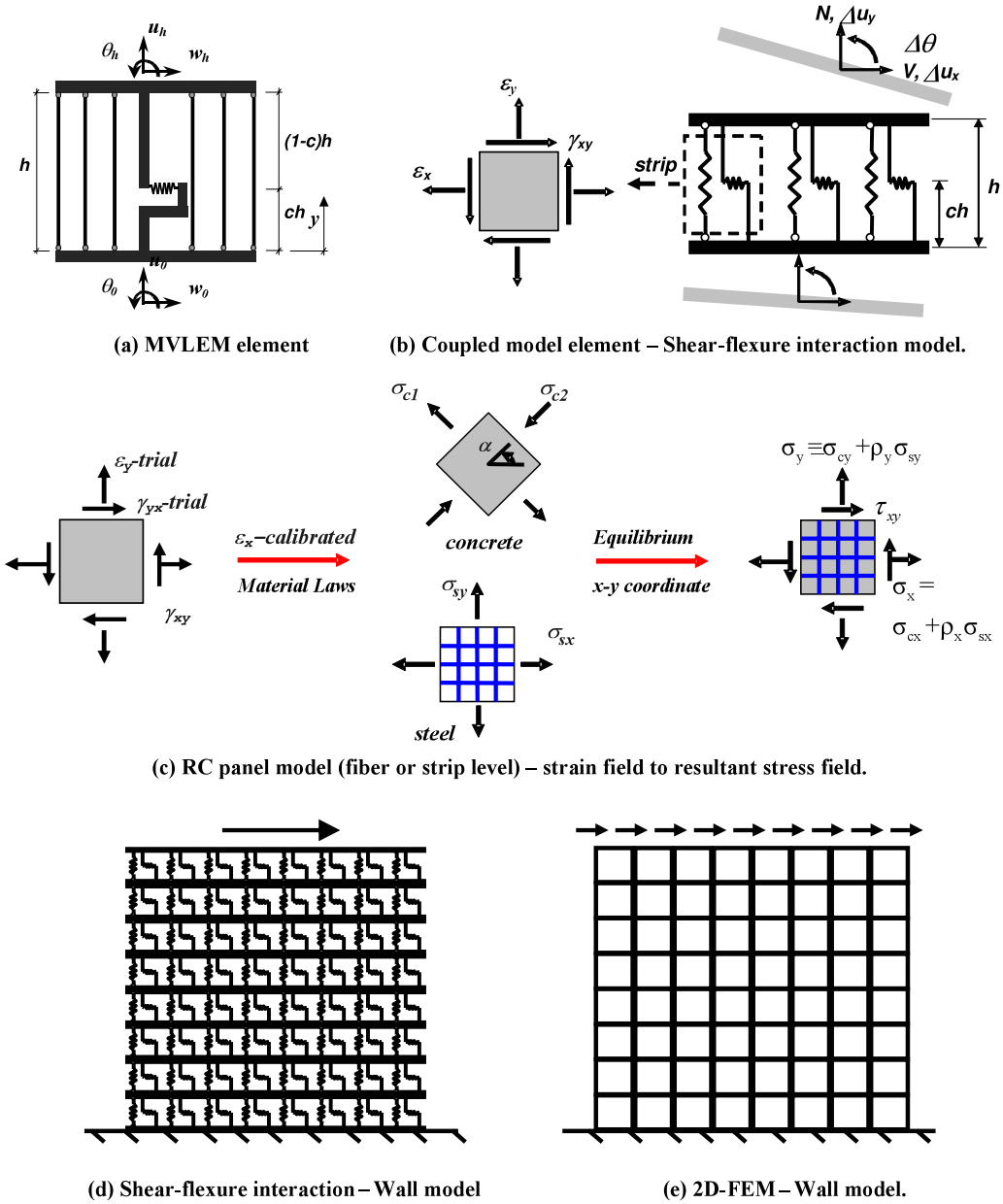

Fig. 1. Element models: (a) MVLEM element, (b) Coupled model element—Shear–flexure interaction model, (c) RC panel model (fiber or strip level)—Strain field to resultant stress field, (d) Shear–flexure interaction—Wall model and (e) 2D-FEM—Wall model.

comparison with test results from heavily instrumented wall segments. Strength predictions, based on the calibrated column-type model, are obtained for a database collected from the literature, resulting in good agreement with experimental evidence.

3. Model description and background

Experimental evidence showed that even for relatively slender wall specimens, shear displacement components provide a much larger and nonlinear contribution than do traditional estimations, using elastic shear response [3,4]. Models that combine flexure and shear can introduce nonlinearity in the shear component, capturing the experimental evidence. An analytical model that combines flexural and shear responses was proposed by Massone et al. [3,5] based on the framework proposed by Petrangeli et al. [6]. The model originally verified for slender elements has also successfully predicted the response of short walls [4,5], although such findings have been validated only for a limited number of specimens. The model formulation, based on a fiber model (e.g., Multiple Vertical Line Element Model, MVLEM [7,8], Fig. 1(a)), involves modifying the traditional uniaxial fiber element by assigning a shear spring to each fiber of the macro-element (Fig. 1(b)). Each modified fiber is then treated as an RC panel element, subjected to in-plane uniform normal and shear stresses (Fig. 1(b)), resulting in the interaction between flexure (contribution of normal/longitudinal stresses) and shear. To represent constitutive panel behavior, a rotating-angle modeling approach such as the Modified Compression Field Theory (MCFT [9]) or the Rotating-Angle Softened-Truss-Model (RA-STM [10]), among other models, can be used. An adaptation of the RA-STM is used in the present study.

For each fiber, based on the constitutive RC panel element, a uniaxial constitutive stress–strain model for concrete is applied along the principal directions to obtain the stress field, assuming that the principal stress and strain directions coincide (Fig. 1(c)). The constitutive relationship employed in the analytical model for concrete considers the effects of biaxial compression softening

(reduction in the principal compressive stresses in concrete due to tensile strains in the orthogonal direction), and tension stiffening (average post-peak tensile stresses in concrete due to the bonding of concrete and reinforcing steel between the cracks). To incorporate the tension stiffening effect into the stress–strain characteristic of concrete, the stress–strain relationship proposed by Belarbi and Hsu [11] is implemented. To describe the stress–strain behavior of concrete in compression, the Thorenfeldt-based curve is calibrated [12,13] and updated by introducing the compression softening parameter proposed by Vecchio and Collins [14]. Reinforcement steel is represented using a uniaxial constitutive stress–strain model along the longitudinal direction of the bars (parallel to x or y directions), assuming perfect bonding between steel and concrete. The reinforcement is modeled using the Menegotto and Pinto model [15], with a softened transition between the initial and post-yield asymptotes accounting for the effects of tension stiffening, that is, softening of the average (smeared) stress–strain relationship of reinforcing bars embedded in concrete (due to concentration of strains in the steel, at crack locations) [11]. More details on the model and material properties are presented elsewhere [3,4].

At the macro-element level, the longitudinal normal (axial) strain (ε_y) and shear distortion (γ_{xy}) components are determined from the six prescribed degrees of freedom (u_x, u_y and θ at both ends of the model element) assuming that the shear strain is uniform along the section and that the plane sections remain plane (Fig. 1(b)). The horizontal or transverse normal strain within each strip or fiber (ε_x) is estimated to complete the definition of the strain field, thus determining the stresses and forces from the constitutive material relationships and geometric properties (dimensions and reinforcement and concrete areas for each strip). The unknown quantity ε_x is numerically solved to achieve the horizontal equilibrium for a given resultant transverse normal stress, σ_x (resultant of horizontal normal stress components in concrete and reinforcing steel). Or, as dealt with in this study, the horizontal normal strains are known (prescribed by a calibrated expression), and therefore this iteration is not necessary. The assembly of several elements stacked one over the other allows wall modeling (e.g., Fig. 1(d) for a cantilever wall with a top lateral load).

Studies by Massone et al. [3,5] revealed that assuming zero horizontal normal strain ($\varepsilon_x = 0$), which may be appropriate for wall specimens with large top and bottom pedestals that constrain lateral expansion, or assuming zero resultant horizontal normal stress ($\sigma_x = 0$) along the entire wall height, which is consistent with boundary conditions at the sides of a wall with no horizontal loads applied over its height, are not capable of correctly reproducing the experimental responses observed in walls with low shear span-to-depth ratios (lower than 0.5). However, the use of an experimentally calibrated expression for the average horizontal normal strain (ε_x) along with a rotational spring to incorporate the reinforcing bar extension within the pedestals resulted in good predictions of lateral force vs. displacement, as well as the contribution of flexure and shear to the top displacement [5]. Such calibration, validated for only a limited number of specimens, cannot necessarily be extended to other specimens with different geometrical and material properties, and a different experimental setup. The following section describes the calibration of the average horizontal normal strain (ε_x) for a variety of test parameters based on a 2D-FEM formulation utilizing the same RC panel material model as the shear–flexure interaction model.

4. Analytical model calibration

To calibrate an average horizontal normal strain to fully complete the strain field of the shear–flexure interaction model, a conventional 2D finite element model (2D-FEM) is formulated. In this study, the wall element is discretized in a series of 4-node rectangular elements that are connected to each other. The 4-node elements use linear interpolation between the nodal displacements and consider reduced integration (one Gauss point at element centroid). The 2D-FEM and shear–flexure interaction models require constitutive laws for the reinforced concrete units, that is, for the 4-node elements and the fibers, respectively. Therefore, for model consistency, the 4-node elements are characterized by the same material models (RC panel behavior) used for the fibers in the shear–flexure interaction model (column-type model); however, in the 2D-FEM case, the horizontal normal strain (ε_x) is part of the equilibrium equations, and therefore no assumptions are required.

The 2D-FEM incorporated the traditional boundary conditions observed for wall tests. Wall specimens are commonly tested under either cantilever condition with a top lateral load, or a double curvature (or zero-end rotation condition) applying a lateral load at specimen mid-height and transferring the load using frames to provide identical moments at both specimen ends (with different sign), or simply applying a lateral load and axial loads to provide the required end moment, resulting in a zero rotation condition at the wall ends. Wall specimens are also generally free to move vertically for a prescribed axial load. To reproduce the boundary conditions, the model was discretized in eight (8) vertical and eight (8) horizontal panels (e.g., Fig. 1(e) for cantilever wall with top lateral load). Further refinement did not modify the overall response significantly. All the nine nodes at wall bottom end were fixed vertically and horizontally, whereas the top nine nodes were forced to move the same prescribed top displacement laterally, assuming there is a constraining effect from the top pedestal. The vertical displacement of the top nodes was differentiated depending on the boundary condition: for cantilever specimens, the vertical displacement moved assuming that the section, which was originally plane, remains plane giving the large rigidity of the top pedestal; and for the double curvature specimens the vertical displacement was set identical for all the nodes.

The model response was analyzed for different parameters, such as: aspect ratio (h_w/ℓ_w), vertical web distributed reinforcement ratio (ρ_{wv}), horizontal web distributed reinforcement ratio (ρ_{wh}), longitudinal boundary reinforcement ratio (ρ_b), axial load (N), compressive strength of concrete (f'_c) and yield strength of steel (f_y). An average horizontal normal strain (ε_x) was obtained at each vertical level by summing the horizontal expansion contribution of all the eight horizontal panel elements and averaged over the wall length. A preliminary analysis revealed that the impact of the material properties (f'_c varying between 30 and 50 MPa, and f_y varying between 280 and 420 MPa) over ε_x was less important than the other parameters (maximum strain values in average varied about 5% and 10% for the extreme values of the material properties of steel and concrete, respectively) given the relatively small range of material property values. For the remaining parameters, a wide range of parameter values was used ($h_w/\ell_w = 1.4, 0.33$; $\rho_{wh} = 0, 1\%$; $\rho_{wv} = 0, 1\%$; $\rho_b = 1, 6\%$; $N = 0, 0.3 f'_c A_g$, where A_g corresponds to the wall cross-sectional area) resulting in 131 cases for analysis, for each boundary condition (262 total cases).

The model results revealed that the average horizontal normal strain (ε_x) reaches its maximum value at wall mid-height in the case of double curvature walls, and normally at a relatively lower location for cantilever walls. The magnitude of the maximum ε_x also increases with the lateral top displacement, which is also considered for the analysis, in terms of drift (δ), that is, the lateral top displacement (Δ) over the height of the wall ($\delta = \Delta/h_w$). All the parameters were incorporated in the analysis by formulating the equation $\varepsilon_x = \varepsilon_{x0}\,(\text{param1})^{\alpha 1} \cdots (\text{paramN})^{\alpha N}$ such that, after applying the least square method, the unknown variables are uniquely determined. Regarding double curvature walls, the calibrated expression for the maximum ε_x, for the most decisive parameters, becomes:

$$\varepsilon_{x,\max} = 0.0033\,(100\rho_h + 0.25)^{-0.53}\left(\frac{h_w}{\ell_w} + 0.5\right)^{0.47}\left(\frac{100N}{f'_c A_g} + 5\right)^{0.25} \cdot (100\delta)^{1.4}. \quad (1)$$

Box I.

The maximum ε_x value occurs at wall mid-height ($\varepsilon_{x,\max} = \varepsilon_x\,(h_w/2)$), whereas the horizontal strain tends to reduce to zero at the wall top and the bottom ends. Although the shape of the average horizontal strain along the height is not the same for all prescribed top lateral displacement, in this study such variation is ignored. Another best-fit analysis is performed, but in this instance a sine function is considered to better represent the average horizontal strain profile, resulting in the following expression,

$$\frac{\varepsilon_x\,(y)}{\varepsilon_{x,\max}} = \sin^{0.75}\left(\frac{y}{h_w}\pi\right) \quad (2)$$

where $\varepsilon_x(y)$ is the average horizontal strain at a specific position (level) along the wall height, y is the distance from that specific position to the bottom boundary of the wall, and h_w is the wall height.

In the case of cantilever walls, the maximum horizontal strain tends to move towards the bottom of the wall ($y < h_w/2$), where the bending moment reaches its maximum value. On an average, the location of maximum horizontal strain occurs at $y = 0.38h_w$, which also varies with drift. Such variation is neglected for simplicity. In this case, the maximum horizontal strain is characterized by,

$$\varepsilon_{x,\max} = 0.0055\,(100\rho_h + 0.25)^{-0.44} \cdot (100\delta)^{1.4}. \quad (3)$$

The same shape is selected in this case to characterize the horizontal strain distribution over the wall height, although the maximum is no longer at wall mid-height. Thus, the expression is modified as,

$$\frac{\varepsilon_x\,(y)}{\varepsilon_{x,\max}} = \begin{cases} \sin^{0.75}\left(\dfrac{y}{0.76h_w}\pi\right) & 0 \le y \le 0.38h_w \\ \sin^{0.75}\left(\dfrac{(y + 0.24h_w)}{1.24h_w}\pi\right) & 0.38h_w < y \le h_w. \end{cases} \quad (4)$$

As mentioned prior, the calibration of the average horizontal strain was performed for a wide range of parameters. However, only a few of them were considered to better represent a characteristic equation for the horizontal strain. Thus, analytical calibration is not intended to obtain an exact or unique expression, but rather a simple, verifiable term. A reasonable estimate of the average horizontal strain was observed [5] to improve the response of the shear–flexure interaction model, even if several assumptions are maintained (e.g., uniform shear strain across the section). Further refinement of an average horizontal strain expression might not necessarily considerably improve the model vs. test response agreement, while maintaining the model assumptions.

In the next two sections, the analytically derived horizontal strain expression is compared with experimental data, as well as the overall response of the walls predicted using the 2D-FEM model in order to validate it.

5. Experimental verification—double curvature tests

Relatively few tests have been instrumented to determine among other things, the average horizontal strain, and therefore only limited information can be included in this section. The specimens described here, are all tested under the double curvature condition having an aspect ratio of about one Box I, and correspond to only a small group of the wide range of wall parameters considered for the model calibration.

5.1. Specimen description and instrumentation

The experimental program carried out at UCLA [4,16] involved testing of 14, lightly reinforced wall pier (WP) and wall spandrel specimens (WS), with dimensions, reinforcement configurations, and material properties selected to represent perimeter wall segments constructed in California, approximately between 1940 and 1970, which included some specific features observed in older buildings. The spandrel specimens were 152 cm tall, 152 cm long, and 15 cm thick, and the piers were 122 cm tall, 137 cm long, and 15 cm thick with a shear span-to-depth ratio ($M/(Vl_w)$) of 0.5 and 0.44, respectively. The shear span-to-depth ratio ($M/(Vl_w)$) is used in this publication to characterize boundary condition effect, such as cantilever walls (zero-end moment condition) or walls under double curvature (zero-end rotation condition), that would reflect the impact of shear in the cases of walls with identical aspect ratio, but different boundary condition. The specimens were tested under the double curvature condition, keeping the bottom and top rotations fixed. The reinforcing steel ratios of the specimens distributed in longitudinal and transverse directions (ρ_l and ρ_t), the corresponding boundary reinforcement ratio (ρ_b), and the axial load levels applied on the specimens during the tests, as well as other specimen characteristics are presented in Table 1 (selected specimens are shown). Four and three test groups, with two identical (companion) specimens in each group, were tested for the wall spandrel (WS) and wall pier (WP) specimen configurations, respectively.

Each test specimen was provided with a very detailed set of instrumentation for post-test studies on model development and validation. DC-LVDTs (DC-excited linear variable differential transducer, referred to as DCDTs) were mounted on the specimens to provide measurements of average deformations at specified locations, to assess, for example, the contribution of shear and flexural deformations to the relative lateral displacement over the specimen height. The average horizontal strain was determined at nine locations: two of them at wall top and bottom ends, and the remaining seven uniformly distributed along the wall height. In this study, only tests 1 to 9 are considered for the analysis, as they included the required instrumentation and were tested under a common protocol. A detailed description of the experimental program and results can be found elsewhere [4,16].

5.2. Load vs. top displacement response

To validate the 2D-FEM model, the overall load vs. displacement response has been studied. All the nine cases are considered and the overall response is estimated for them all. An earlier work showed that the rebar extension (strain penetration) within the pedestal could influence the response prediction, due to the additional flexibility of this effect [5]. An estimated top displacement was removed from the experimental top lateral displacement as explained by Massone et al. [5], based on cumulative displacement as strain penetrates into the pedestal and sectional analysis. Such corrections generally resulted in about 10% reduction of the top displacement at peak lateral force.

Fig. 2 shows the overall lateral force vs. lateral top displacement for test 1 and test 6 for the 2D-FEM model and experimental results. Regarding the experimental results, an envelope of all the cycles is shown. Analysis is performed until significant degradation is observed, because damage localization could result in an

Table 1
Properties of wall specimens.

Test no.	t_w (cm)	l_w (cm)	h_w (cm)	Reinforcement				Axial load	Material properties			Shear strength		
				ρ_t (%)[b]	ρ_l (%)[b]	Boundary		N/A$_g f'_c$ (%)	f'_c (MPa)	f_y, ϕ13[a] (MPa)	f_y, ϕ16[a] (MPa)	$V_{n,\text{exp}}$ (kN)	$V_{n,\text{2D-FEM}}$ (kN)	$\frac{V_{n,\text{2D-FEM}}}{V_{n,\text{exp}}}$
						Rebar[a]	ρ_b(%)							
test1	15.2	152	152	0.278	0.428	4-ϕ16	3.12	0	25.5	424.0	448.2	633	623	0.98
test4	15.2	152	152	0.278	0.428	4-ϕ16	3.12	0	43.7	424.0	448.2	749	749	1.00
test2	15.2	152	152	0.278	0.400	1-ϕ13 + 1-ϕ16	1.70	0	31.4	424.0	448.2	453	538	1.19
test3	15.2	152	152	0.278	0.400	1-ϕ13 + 1-ϕ16	1.70	0	31.0	424.0	448.2	491	536	1.09
test9	15.2	137	122	0.278	0.227	2-ϕ13	1.33	0	29.9	424.0	–	404	443	1.10
test7	15.2	137	122	0.278	0.227	2-ϕ13	1.33	5	31.9	424.0	–	648	634	0.98
test8	15.2	137	122	0.278	0.227	2-ϕ13	1.33	5	32.0	424.0	–	682	634	0.93
test5	15.2	137	122	0.278	0.227	2-ϕ13	1.33	10	28.3	424.0	–	753	706	0.94
test6	15.2	137	122	0.278	0.227	2-ϕ13	1.33	10	31.4	424.0	–	819	753	0.92
													AVG	1.01
													STD	0.09

Conversion factors: 1 cm = 0.394 in., 1 kN = 0.225 kips, 1 MPa = 0.145 ksi.
[a] Ribbed ϕ13 (13 mm diameter) = US #4; ribbed ϕ16 (16 mm diameter) = US #5.
[b] All reinforcement bars were ϕ13.

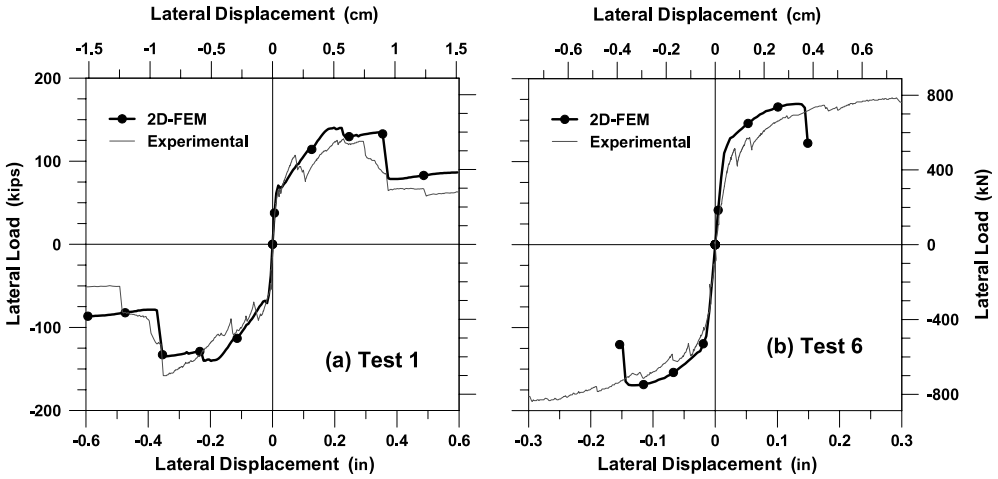

Fig. 2. Load vs. top displacement: (a) Test 1, and (b) Test 6.

inaccurate post-peak response. The analytical result recovers the general shape of the test results, that is, the initial stiffness and strength. All other specimens reveal similar trends (not shown). In Table 1, the shear capacity estimate ($V_{n,\text{2D-FEM}}$) is compared with the average (positive and negative directions) experimental shear capacity ($V_{n,\text{exp}}$), indicating that generally a difference lower than 10% exists between the prediction and the experimental observation, and that the $V_{n,\text{2D-FEM}}/V_{n,\text{exp}}$ ratio shows an average of 1.01 and a coefficient of variation of 0.09 for all the nine specimens. As explained later, after the calibrated average horizontal strain function (calibrated from the 2D-FEM) was implemented into the shear–flexure interaction model, the shear strength ratio yielded a value of 0.97, with a coefficient of variation of 0.12, which reveals that the 2D-FEM model better captures the wall shear strength, although the differences are relatively small. A similar analysis performed by Massone et al. [5] considered a different condition for the horizontal equilibrium: (1) zero horizontal stress resultant and (2) zero horizontal strain value. Such cases were regarded as extreme situations and imposed at the fiber level, which resulted in under-predictions of the shear strength for the zero stress case, and over-predictions of the shear strength for the zero strain case, with a difference of about 30% on average, with similar or even larger coefficients of variation. Among others, the shear–flexure interaction model has assumptions not considered in the 2D-FEM model, which are: (1) plane sections remain plane after loading, (2) constant (uniform) horizontal strain values used across the section, and (3) uniform shear strain across the section. The small strength difference (and coefficient of variation) between the 2D-FEM and the shear–flexure interaction model, and its closeness to the experimental evidence suggests that the impact of such assumptions have less influence than offering a reasonably accurate average horizontal strain prediction for walls. Thus, the shear–flexure interaction model accurately reproduces experimental behavior, been at the same time more suitable for implementation and system studies.

On closer study, the overall response for the shear–flexure interaction model by separating the top displacement between flexural and shear contribution, generally reveals the flexural contribution to usually account for about 30%–40% of the top displacement at small drift levels (up to 0.05%–0.1% drift), which decreases to about 10% when lateral load capacity is reached (usually over 0.4% drift). This is consistent with the experimental evidence [5] (after removing the predicted flexibility due to rebar extension within the pedestal). Significantly, the small shear span-to-depth ratio (about 0.5) increases the importance of the shear displacement component (90% at a large displacement); however, at the small drift levels, the flexural response (30%–40%) observed cannot be ignored. Thus, using a model that can account for both deformation components is essential to predict stiffness and strength correctly.

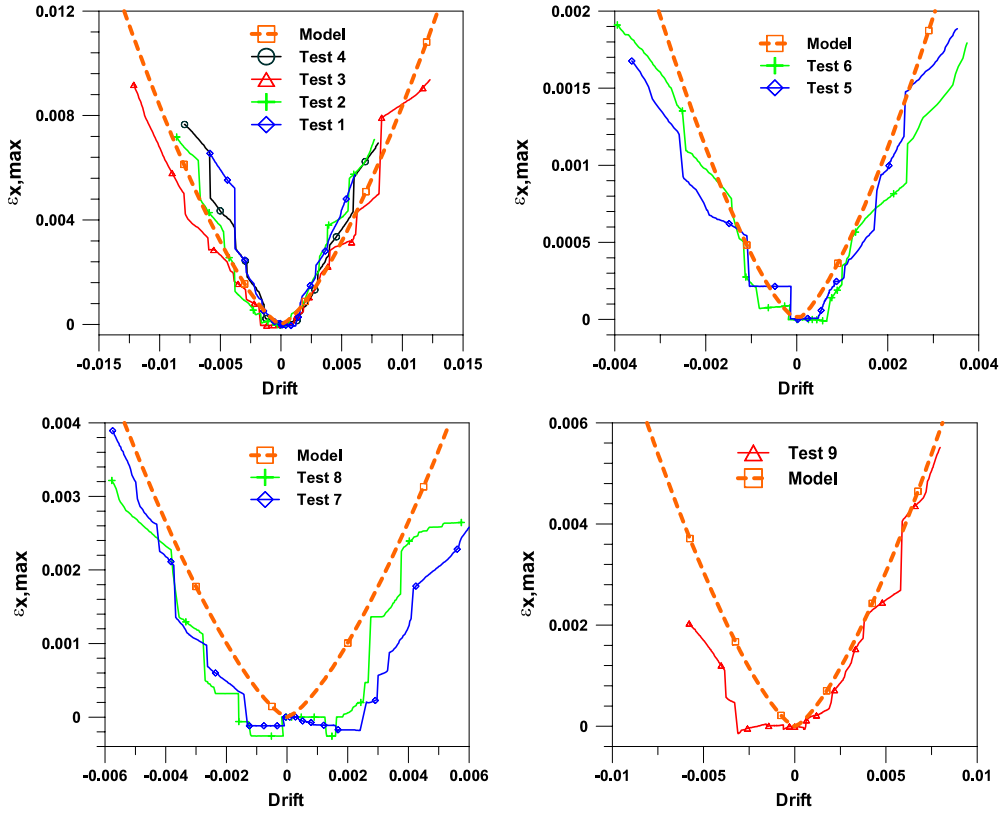

Fig. 3. Average horizontal strains vs. drift.

5.3. Maximum average transverse strain

Fig. 3 shows the experimental and analytical (calibrated) maximum (at wall mid-height) average horizontal strain for all the nine specimens. The variation of ε_x with drift is seen for most cases; however, there is a tendency to overestimate the strain values for the specimens with axial load (test 5 to test 8).

5.4. Average transverse strain profile

Fig. 4(a) and (b) show the experimental and analytical (calibrated) average horizontal strain profile, that is, the measured strain values at all the nine locations and the model predictions (calibrated ε_x) for two specimens (test 3 and test 5). Test 3 (Fig. 4(a)) was the only specimen where the sensors on the specimens were removed after relatively large drift values (1.2%). The drift values depicted in the figures correspond to the nominal value, before the correction due to rebar extension within the pedestals. The analytical magnitude and shape of the strain profile recover the experimental evidence in test 3 reasonably well. In test 5 (Fig. 4(b)), as mentioned earlier on, the model over-estimates the mid-height strain values (specimen with axial load), although given that the maximum value for this particular test occurs at a lower location, that overestimation appears less significant.

6. Experimental verification—cantilever wall tests

Maier and Thürlimann [17] conducted one of the few wall test programs that considered a robust instrumentation layout for cantilever walls, consisting of a series of 10 walls with an aspect ratio of 1.02, and a variation of boundary types, reinforcement ratios and axial loads. Only one of them is described here for comparison purposes (specimen S2).

6.1. Specimen description and instrumentation

Specimen S2, with a flanged cross-section, was monotonically loaded under a cantilever loading condition with a lateral point load applied at the wall top. The specimen was 1.2 m high, 1.18 m long (boundary element length included) and 0.1 m thick. The boundary elements were 0.4 m long and 0.1 m thick. Uniform web reinforcement producing a web reinforcing ratio of 1% was included vertically and horizontally. The boundaries were reinforced with a 1.26% boundary longitudinal reinforcement ratio. The compressive concrete capacity was 36.9 MPa and the yield stress of the reinforcement was 574 MPa. The specimen was loaded with a constant axial load of about $0.25A_g f'_c$ (where A_g corresponds to the total cross-section area).

Vertical and horizontal relative displacements were measured at 63 points along the wall web (9 rows and 7 columns), and horizontal strain values were calculated from the horizontal displacement measurements obtained at each mesh point. The average along the length of the wall resulted in the average measured horizontal strain distributions for the nine height levels.

6.2. Average transverse strain profile

Fig. 4(c) shows the average horizontal strain at different levels for three different loads or drift levels ($\delta = 0.65\%$ at approximately wall maximum capacity, $\delta = 0.14\%$ at approximately wall first yield and $\delta = 0.34\%$, an intermediate drift case). The drift values were approximately estimated as no correction is originally included by pedestal rotation, or because the relative horizontal displacement is given between the top and bottom pedestal instead of within the wall zone. The top displacement was corrected by subtracting the relative rotation observed between the overall wall specimen (including top and bottom pedestal) and the wall section, and assuming that rigid body rotation due to this movement would generate a top displacement that does not correspond

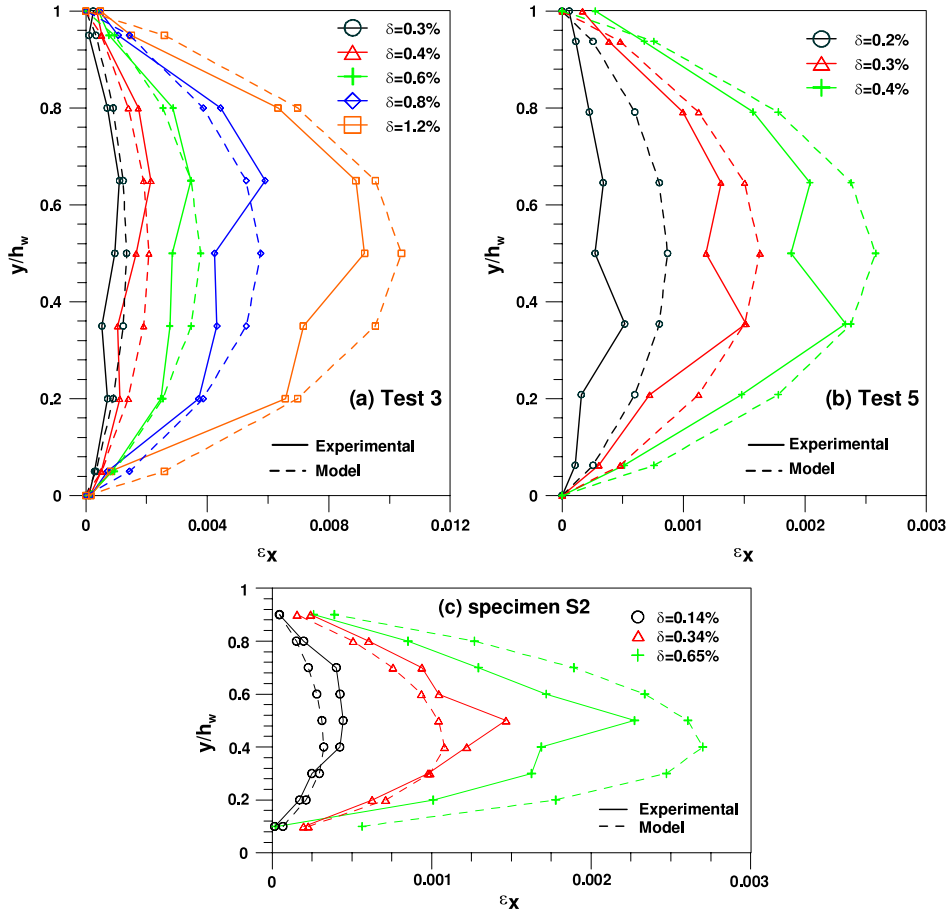

Fig. 4. Average horizontal strain profiles: (a) Test 3, (b) Test 5 and (c) Specimen S2.

to actual deformation of the wall section. Therefore, in the discussion that follows, the focus is on the overall response rather than on specific strain values. As evident in the experimental results, the horizontal strain rapidly reduces from its maximum value close to the central zone level towards both ends (top and bottom), as predicted by the calibrated expression (model), reproducing the shape of the strain distribution, as well as the magnitude at different drift levels, reasonably well.

7. Shear strength test database comparison

The earlier sections validated the response observed using the 2D-FEM model, which generates the calibrated expression for the average horizontal normal strain (ε_x). This expression is now used in the shear–flexure interaction model, and validated by comparing the strength prediction with a large collection of wall test data reported in the literature. The strength predictions are also comparatively studied with a common expression from the ACI 318-08 [1] code. Thus, strength and dispersion of such prediction, as well as dependency to model parameters can be revised.

A database of relevant test results (252 specimens) was collected by reviewing the available research, including work summarized by Hirosawa [18] and Mohammadi-Doostdar and Saatcioglu [19], and the publications by Massone et al. [5], Hidalgo et al. [20], Yamada et al. [21], Antebi et al. [22], Barda et al. [23], Benjamin and Williams [24], Cardenas et al. [25], and Galletly [26]. The database includes walls with enlarged end sections such as flanged or barbell section (68%) and rectangular cross-sections (32%). The wall specimens were tested either as cantilever walls with a top point load (under single curvature, 85%) or under a fixed rotation condition at both ends by either applying an external moment or imposing zero rotation at the wall ends (under double curvature, 15%). The longitudinal reinforcement boundary ratio for the test specimens in the database ranged between 0.7% and 11% measured over the boundary cross-section (enlarged section in the case of barbell walls and 10% of the cross-section for rectangular walls); the longitudinal and transverse web reinforcement ratios varied between 0% and 3.7%, and the yield strength of all reinforcing bars ranged between 209 MPa and 624 MPa. The concrete compressive strength varied between 12.4 MPa and 63.4 MPa. The axial load, although applied in a few cases (axial load greater than $0.01 f_c' l_w t_w$, 15%) reached values of $0.27 f_c' l_w t_w$, where l_w and t_w are the length and thickness of the wall, respectively. The shear span-to-depth ratio ($M/(Vl_w)$) varied between 0.29 and 2, which was similar for the wall aspect ratio (h_w/l_w).

Shear strength is also determined based on the ACI 318-08 [1] code (Equation 21-7), as $V_n = A_{cv}(\alpha_c \lambda \sqrt{f_c'} + \rho_t f_y)$, where the coefficient λ is 1.0 for normal-weight concrete, and α_c is 0.25 (f_c' in MPa) for $h_w/l_w \leq 1.5$, and is 0.17 for $h_w/l_w \geq 2.0$, and linearly interpolated between the limit aspect ratios. A_{cv} represents the cross-sectional web area of a wall, ρ_t is the transverse reinforcement ratio, f_y is the yield strength of the transverse reinforcement, and f_c' is the compressive strength of concrete. The nominal shear strength for individual walls cannot be greater than $0.83 A_{cw} \sqrt{f_c'(\text{MPa})}$ where A_{cw} represents the entire cross-sectional area of the wall.

All the 252 specimens were modeled using the interaction model, assuming a fixed condition at the wall base and laterally loaded with a point load. The specimens tested under cantilever condition were free to rotate at wall top end, whereas for the specimens loaded under double curvature condition, a zero rotation

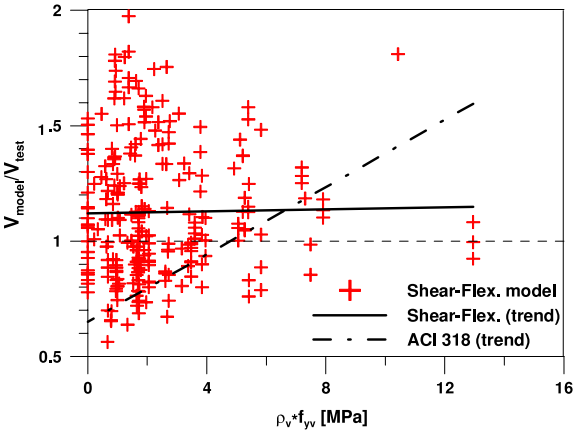

Fig. 5. Shear strength ratio (V_{model}/V_{test}) vs. vertical web reinforcement.

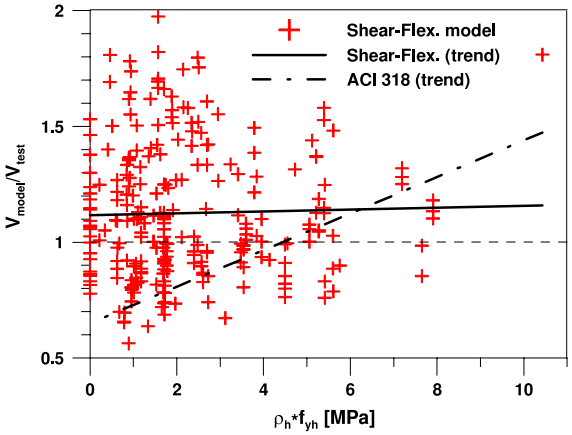

Fig. 6. Shear strength ratio (V_{model}/V_{test}) vs. horizontal web reinforcement.

condition was imposed. The wall models were discretized in eight elements and eight fibers, and the same material models as for the 2D-FEM model were used, and calibrated with the as-tested material properties. The shear strength, that is, the maximum lateral force attained was obtained by performing a top displacement control analysis for all the wall cases, and comparing with the observed (experimental) shear strength.

The ratio of the predicted over the experimental shear strength, or strength ratio, was determined for all cases (V_{model}/V_{exp}). The average strength ratio for the shear–flexure interaction model for all the wall specimens was 1.13, with a coefficient of variation of 0.25, indicating a reasonably good correlation with the test results, and a relatively small dispersion. The maximum and minimum strength ratios were 1.97 and 0.56, respectively, although the majority of them ranged between 1.6 and 0.7 (89%). Identical analysis was performed with the ACI 318-08 shear strength equation; however, in this instance, a few cases that were expected to have a flexural failure were removed. To estimate the flexural capacity (M_n) a sectional analysis was performed, according to ACI 318 (Section 10) recommendations. Based on the moment or flexural capacity, the shear force required to reach such a moment was estimated and compared with the shear strength of a shear failure (V_n) to clearly distinguish possible flexural failure from shear failure. Thus, only cases controlled by shear failure (according to this analysis) were considered to eliminate distortions in the analysis either from tests expected to fail in flexure or an expression estimating flexural capacity. These cases were maintained for the shear–flexure interaction model to validate the ability of such a model to also predict their shear strength. Thus, for the ACI 318 equation, the number of tests was reduced to 205 (81% of the original database). The average strength ratio for the ACI 318 expression was 0.80, with a coefficient of variation of 0.37, which indicates a much larger dispersion than the shear–flexure interaction model, although the model tends to be more conservative. The maximum and minimum strength ratios were 1.93 and 0.21, respectively, although in this case the majority ranged between 1.3 and 0.3 (93%). It is important to indicate that the strength ratio (V_{model}/V_{exp}) was selected to have in the numerator the model capacity to correlate such value, normalized to the observed strength, to wall parameters. Taking the inverse of the strength ratio definition (V_{exp}/V_{model}) would show similar extreme values for the interaction model (0.51 to 1.77) and identical coefficient of variation. On the contrary, the ACI expression would reveal a much larger range (0.52 to 4.74) and a larger coefficient of variation (0.48), given that the ACI expression is intended to be conservative.

Although the shear–flexure interaction model presents good correlation of the shear strength with test results, it is interesting to observe if the model adequately predicts the shear strength for different values of the model parameters. Thus, this enables investigating if the model can correctly predict increments or decrements of shear strength to parameter variations. Considering that most tests correspond to different experimental programs and that identical specimens with only one variable variation are few, a sensitivity analysis of the shear strength ratio (V_{model}/V_{exp}) to different model parameter variables to the entire database was performed. Steel reinforcing ratios, concrete compressive strength, level of axial load, cross-section type, boundary condition, shear span-to-depth ratio, and observed average shear stress are considered for the sensitivity analysis (Figs. 5–12).

In Figs. 5–12 a dotted line indicates the perfect correlation between the model and the tests ($V_{model}/V_{test} = 1$). The general trend is characterized by a linear best-fit analysis of the data, with respect to different variables. Although only the data obtained for the shear–flexure interaction model is shown (Figs. 5–12(a), and only Fig. 12(b) shows the ACI 318 prediction data), the linear trend is also presented for the shear strength prediction with the ACI 318 expression in all the figures.

7.1. Sensitivity—vertical and horizontal web reinforcement ratio

Figs. 5 and 6 show the model prediction sensitivity to the vertical and horizontal reinforcing steel ratio times its yield strength. The yield strength was incorporated into the parameter to account for the force that the steel can develop per unit area rather than just the steel ratio. The general trend (linear) indicates that there is little correlation of the observed strength ratio obtained with the shear–flexure interaction model and the vertical or horizontal reinforcement, indicating that such parameter variations are well captured with the model. On the contrary, the linear trend obtained with the ACI 318 strength equation is highly dependent on both the variables, with differences in prediction up to about 80% for the overall range.

7.2. Sensitivity—longitudinal boundary reinforcement ratio

Fig. 7 shows the model prediction sensitivity to the longitudinal boundary reinforcing steel ratio times its yield strength. The general trend (linear) shows relatively small dependency on such a parameter (about 10% variation over the whole range) when considering the shear–flexure interaction model, as well as the ACI 318 strength prediction. This indicates that because the ACI 318 strength equation is not dependent on the amount of boundary reinforcement it is only relevant to predict the lateral strength for flexural failure. This supports the idea that the specimens, although they could have been influenced by flexural response, such an influence is not relevant to estimate the shear strength using the ACI 318 equation.

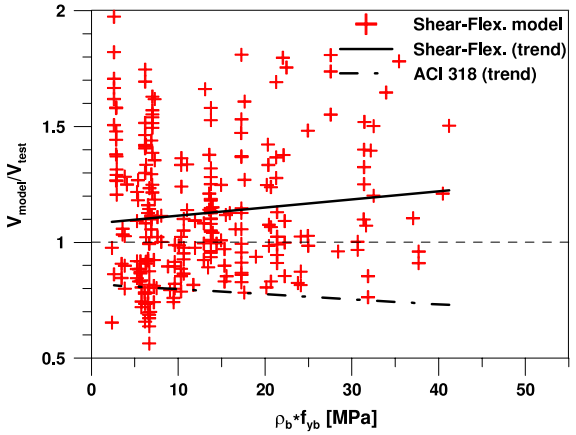

Fig. 7. Shear strength ratio (V_{model}/V_{test}) vs. longitudinal boundary reinforcement.

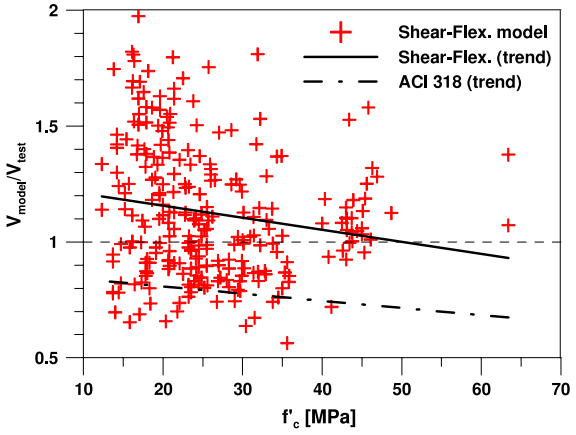

Fig. 8. Shear strength ratio (V_{model}/V_{test}) vs. concrete compressive strength.

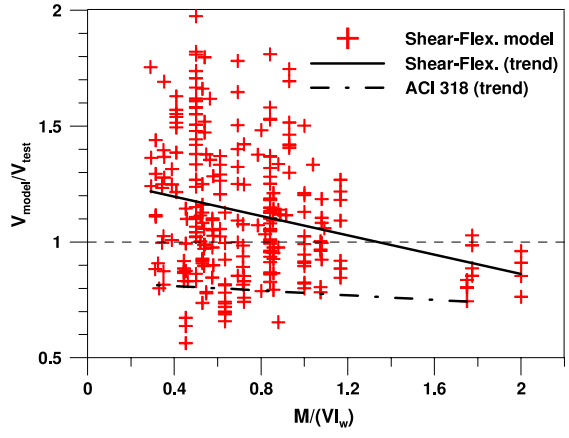

Fig. 9. Shear strength ratio (V_{model}/V_{test}) vs. shear span-to-depth ratio.

7.3. Sensitivity—concrete compressive strength and shear span-to-depth ratio

Figs. 8 and 9 show the model prediction sensitivity to the concrete compressive strength and shear span-to-depth ratio, respectively. The general trend (linear) indicates an important dependency on both parameters (about 30% variation over the whole range) when considering the shear–flexure interaction model, resulting in over-predictions for small compressive strength values, as well as for small shear span-to-depth ratio values. The ACI 318 strength prediction equation is less dependent on both parameters (almost insensitive to shear span-to-depth ratio). The important differences observed in the interaction model compared with the ACI expression in the case of shear span-to-depth ratio (Fig. 9) are partly because of the specimens considered for the interaction model that are not considered for the ACI expression. As these specimens are assumed to have flexural failure, and therefore with a tendency towards a larger shear span-to-depth ratio, they are placed to the right of the figure. Such cases show conservative values of the strength ratio, promoting a negative slope of the trend line (shear–flexure interaction model). The ACI expression, already conservative, includes a few specimens with a large shear span-to-depth ratio (trend line rises up to $M/(Vl_w) = 1.75$ for the ACI and $M/(Vl_w) = 2.0$ for the interaction model) resulting in a decreased impact to sensitivity in this parameter.

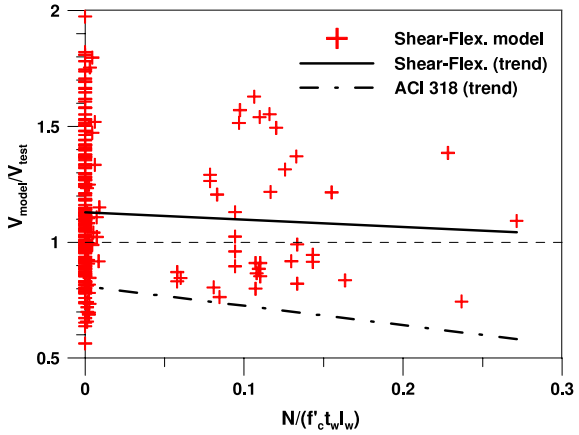

Fig. 10. Shear strength ratio (V_{model}/V_{test}) vs. axial load level.

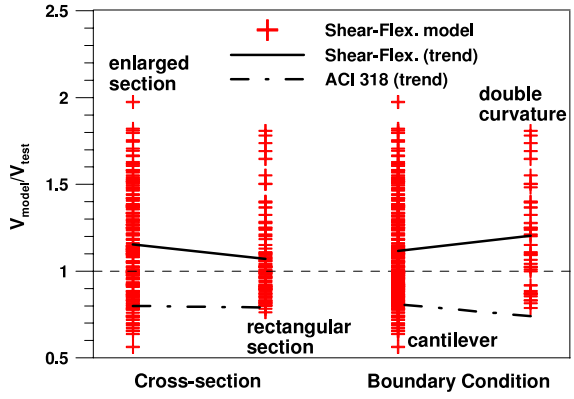

Fig. 11. Shear strength ratio (V_{model}/V_{test}) vs. cross-sectional shape and boundary condition.

7.4. Sensitivity—axial load

Fig. 10 shows the model prediction sensitivity to the level of axial load. Although there are only a few specimens with an axial load higher than $0.01 f_c' t_w l_w$ (15% of the database), the general trend (linear) shows little dependency to such a parameter (less than 10% variation over the whole range) when considering the shear–flexure interaction model. On the contrary, the ACI 318 strength equation results in an under-prediction of the shear strength (over 20% variation for the whole range), especially for specimens with high axial load, consistent with the fact that such expression does not account for shear strength improvement with axial load.

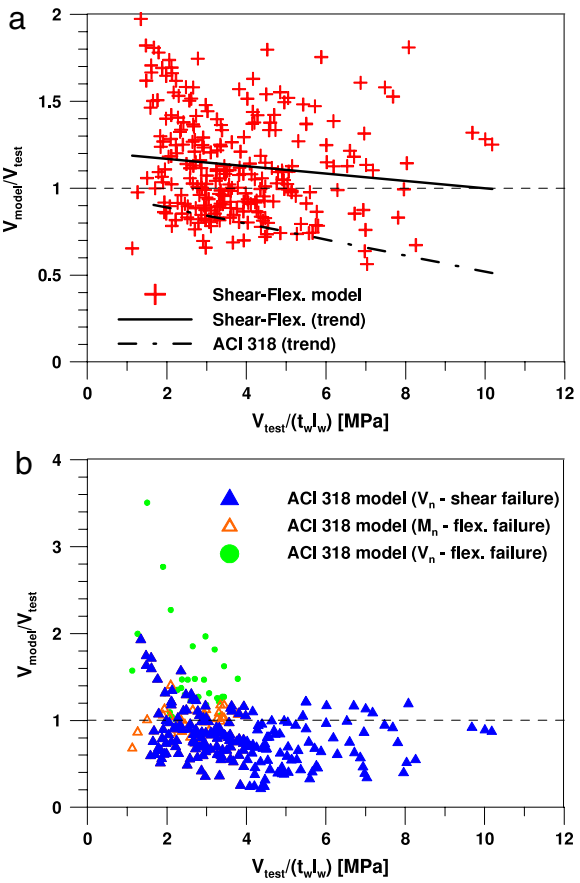

Fig. 12. Shear strength ratio (V_{model}/V_{test}) vs. experimental shear stress: (a) shear–flexure interaction model, and (b) ACI 318.

7.5. Sensitivity—wall shape and boundary condition

Fig. 11 shows the model prediction sensitivity to the cross-sectional wall shape and boundary condition. The results reveal that the average strength ratio for rectangular and enlarged cross-section walls (barbell and flanged walls), as well as walls in the cantilever condition (single curvature) and double curvature (zero-end rotation) is similar for the shear–flexure interaction model as well as for the ACI 318 strength equation, indicating observation of no cross-sectional shape nor boundary condition dependency.

7.6. Sensitivity—average observed (experimental) shear stress

Fig. 12 shows the model prediction sensitivity to the average observed (experimental) shear stress. Although this value is not a model parameter, the comparison is included to verify if the model is capable of reproducing the shear strength for walls under low and high shear stress levels. Fig. 12(a) includes the analytical results for the shear–flexure interaction model, as well as its linear trend, and the linear trend obtained for the ACI 318 strength equation. Fig. 12(b) includes the analytical results for the ACI 318 strength equation. In this instance, the entire test database was included (252 specimens), that is, the tests expected to show flexural failure were also considered (47 specimens), although different symbology was used (flexural failure and shear failure differentiated). Shear capacity of specimens expected to show shear failure were determined based on the shear strength prediction (V_n), whereas the specimens expected to fail in flexure were determined based on the moment capacity (M_n). Additionally, the shear capacity based on the shear strength prediction is also included for comparison, for those expected to show flexural failure.

The strength ratio for the shear–flexure interaction model reveals some dependency to the observed average shear stress (about 20% variation over the whole range), whereas the ACI 318 strength equation shows a variation of about 40% over the entire shear stress range (Fig. 12(a)). Such dependency is even more pronounced (about 70% over the entire shear stress range—not shown) when the shear strength ratio is investigated for the entire database without distinguishing between shear and flexural failure (shear strength based on V_n, Fig. 12(b)). Large over-predictions are observed for specimens likely to fail in flexure (experimental average shear stress values lower than 4 MPa), but with shear capacity estimated based on the shear strength equation (V_n), which are partially corrected when the strength is based on flexural capacity (M_n). Over-predictions are expected as a different mode of failure governs the response. This might indicate that the ACI 318 strength equation, with a 40% variation of its trend line, fails to correctly capture the walls' failure mode and therefore their capacity, even when the specimens are expected to show shear failure, as seen in Fig. 12(a). The shear–flexure interaction model could reveal a similar situation, although the dependency is about half the value observed with the ACI 318 expression.

8. Summary and conclusions

This study investigated, verified and generalized a modeling approach integrating flexure and shear interaction to reasonably predict the inelastic response of reinforced concrete squat walls. The model incorporates RC panel behavior into a displacement-based column model by prescribing the average horizontal strain (ε_x) at different wall heights. The average horizontal strain equation is calibrated using a 2D-FEM model that incorporated identical RC panel behavior, but in this case satisfying the equilibrium allowed, thus generalizing the expressions for the strain. The analytical study of 262 cases, where the variation of aspect ratio, vertically and horizontally distributed web reinforcement ratio, longitudinal boundary reinforcement ratio and axial load level, as well as the boundary condition (cantilever and zero-end rotation), were performed to propose an analytical expression to estimate the average horizontal strain. An experimental program was used to verify the proposed expressions, although only a limited number of specimens was considered, and therefore, only a limited range of variables were compared. To improve the validity of the analytical model, a database was assembled for relatively short walls (aspect ratio lower than 2) with predominant shear failure. The model shear strength, that is, the maximum lateral wall capacity was compared to the database, as well as the prediction estimated using the ACI 318 code.

The analytical evidence, based on the 2D-FEM formulation, indicates that the average horizontal strain is mainly dependent on parameters such as: aspect ratio, horizontally distributed web reinforcement ratio, and axial load level, as well as lateral drift. The experimental evidence shows relatively good correlation to the analytical expressions when considering the variation of the maximum strain with the drift and the strain distribution over the wall height.

Comparisons with a database involving 252 wall specimens resulted in an average ratio of the predicted over the experimental shear strength (V_{model}/V_{exp}) of 1.13 for all the cases for the shear–flexure interaction model with a coefficient of variation of 0.25, indicating a reasonably good correlation with tests results; however, for the ACI 318-08 shear strength equation, the average strength ratio was 0.80 with a coefficient of variation of 0.37, for a reduced database (expected flexural-dominated specimens were removed, reducing the database by 19%).

A sensitivity study, based on a linear trend estimation, indicates that the shear–flexure interaction model strength prediction

ratio, that is, the model over the experimental strength value, is almost nil sensitive to the vertical and horizontal web reinforcement strength ratio, and to the longitudinal boundary reinforcement strength ratio, cross-sectional shape (rectangular or enlarged section), boundary condition (cantilever or zero-end rotation condition) and axial load level (generally less than 10% variation over the whole range). More significant dependency is observed in the shear–flexure interaction model to the shear span-to-depth ratio, compressive concrete strength and experimental shear stress.

Thus, the shear–flexure interaction is a mechanical model that, with an adequate calibration of the average horizontal strain, not only results in reasonable good strength predictions, but also in a more consistent response, whose strength ratio is not as sensitive to model parameters as the ACI 318 expression, even if assumptions such as: plane section remain plane, constant horizontal normal and shear strain across the section are maintained. Besides, the shear–flexure interaction model is also capable of giving load vs. displacement response (this study focuses on strength prediction), as well as other information such as flexural and shear contribution to top displacement, important for performance assessment.

Acknowledgements

Financial support for this project provided by Chile's National Commission on Scientific and Technological Research (CONICYT) for the project Fondecyt 2008, Initiation into Research Funding Competition, under Grant No. 11080010, is gratefully acknowledged. The comments and suggestions by Dr. Kutay Orakçal from Boğaziçi University on the draft of the paper are greatly appreciated.

References

[1] ACI 318-08: Building code requirements for structural concrete and commentary. Committee 318. Farmington Hills (Michigan): American Concrete Institute; 2008. p. 467.
[2] Massone LM, Wallace JW. Load—Deformation responses of slender reinforced concrete walls. ACI Struct J 2004;101(1):103–13.
[3] Massone LM, Orakcal K, Wallace JW. Shear–flexure interaction for structural walls. SP-236. ACI special publication—Deformation capacity and shear strength of reinforced concrete members under cyclic loading. 2006. p. 127–50.
[4] Massone LM. RC wall shear–flexure interaction: Analytical and experimental responses. Ph.D. dissertation. Los Angeles: University of California; 2006. p. 398.
[5] Massone LM, Orakcal K, Wallace JW. Modeling of squat structural walls controlled by shear. ACI Struct J 2009;106(5):646–55.
[6] Petrangeli M, Pinto PE, Ciampi V. Fiber element for cyclic bending and shear of RC structures. I: Theory. J Eng Mech 1999;125(9):994–1001.
[7] Vulcano A, Bertero VV, Colotti V. Analytical modeling of RC structural walls. In: Proceedings, 9th world conference on earthquake engineering. vol. 6. 1988. p. 41–6.
[8] Orakcal K, Wallace JW, Conte JP. Nonlinear modeling and analysis of slender reinforced concrete walls. ACI Struct J 2004;101(5):688–99.
[9] Vecchio FJ, Collins MP. The modified compression-field theory for reinforced concrete elements subjected to shear. ACI J 1986;83(2):219–31.
[10] Pang XD, Hsu TTC. Behavior of reinforced concrete membrane elements in shear. ACI Struct J 1995;92(6):665–79.
[11] Belarbi H, Hsu TCC. Constitutive laws of concrete in tension and reinforcing bars stiffened by concrete. ACI Struct J 1994;91(4):465–74.
[12] Collins MP, Porasz A. Shear strength for high strength concrete. Bull. no. 193—Design aspects of high strength concrete. Comite Euro-International du Beton (CEB); 1989. p. 75–83.
[13] Carreira DJ, Kuang-Han C. Stress–strain relationship for plain concrete in compression. ACI Struct J 1985;82(6):797–804.
[14] Vecchio FJ, Collins MP. Compression response of cracked reinforced concrete. J Struct Eng 1993;119(12):3590–610.
[15] Menegotto M, Pinto E. Method of analysis for cyclically loaded reinforced concrete plane frames including changes in geometry and non-elastic behavior of elements under combined normal force and bending. In: Proceedings, IABSE symposium. 1973. p. 15–21.
[16] Orakcal K, Massone LM, Wallace JW. Shear strength of lightly reinforced wall piers and spandrels. ACI Struct J 2009;106(4):455–65.
[17] Maier J, Thürlimann B. Bruchversuche an stahlbetonsheiben. Institut fur Baustalik and Konstruktion. Zurich (Germany): Eidgenossische Technische Hochschule Zurich; 1985. p. 130 [in German].
[18] Hirosawa M. Past experimental results on reinforced concrete shear walls and their analysis. Kenchiku Kenkyu Shiryo. No. 6. Tokyo: Building Research Institute, Ministry of Construction; 1975. p. 277 [in Japanese].
[19] Mohammadi-Doostdar H, Saatcioglu M. Behavior and design of earthquake resistant low-rise shear walls. Report OCCERC 02-28. Ottawa Carleton Earthquake Engineering Research Center. Canada: Department of Civil Eng., University of Ottawa; 2002. p. 250.
[20] Hidalgo PA, Ledezma CA, Jordan RM. Seismic behavior of squat reinforced concrete shear walls. Earthq Spectra 2002;18(2):287–308.
[21] Yamada M, Kawamura H, Katagihara K. Reinforced concrete shear walls without openings; test and analysis. SP-42. ACI special publication—Shear in reinforced concrete. 1974. p. 539–58.
[22] Antebi J, Utku S, Hansen RJ. The response of shear walls to dynamic loads. Cambridge: Department of Civil and Sanitary Eng., Massachusetts Institute of Technology; August 1960. p. 177.
[23] Barda F, Hanson JM, Corley WG. Shear strength of low-rise walls with boundary elements. SP-53. ACI special publication—Reinforced concrete structures in seismic zones. 1977. p. 149–202.
[24] Benjamin JR, Williams HA. The behavior of one-story reinforced concrete shear walls. J Struct Div, ASCE 1957;83(3):1–49.
[25] Cardenas AE, Russell HG, Corley WG. Strength of low-rise structural walls. SP-63. ACI special publication—Reinforced concrete structures subject to wind and earthquake forces. 1980. p. 221–41.
[26] Galletly GD. Behavior of reinforced concrete shear walls under static load. Cambridge: Department of Civil and Sanitary Eng., Massachusetts Institute of Technology; August 1952. p. 123.